Journal of Hydrology: Regional Studies 40 (2022) 101037

Contents lists available at ScienceDirect

Journal of Hydrology: Regional Studies

journal homepage: www.elsevier.com/locate/ejrh

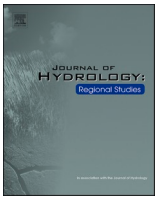

Assessing rainfall global products reliability for water resource management in a tropical volcanic mountainous catchment

M. Dumont [a,*], M. Saadi [a], L. Oudin [a], P. Lachassagne [b], B. Nugraha [c], A. Fadillah [d], J.-L. Bonjour [e], A. Muhammad [d], Hendarmawan [c], N. Dörfliger [e], V. Plagnes [a]

[a] Sorbonne Université, CNRS, EPHE, UMR 7619 METIS, F-75005 Paris, France
[b] HSM, Univ. Montpellier, CNRS, IMT Mines Alès, IRD, Montpellier, France
[c] Faculty of Geological Engineering, Universitas Padjadjaran, Jatinangor, Sumedang 45363, Indonesia
[d] Danone Aqua group, Department of Water Resources, Jakarta, Indonesia
[e] Water Institute by Evian, Water Resources and Sustainability Division, Danone Waters, Evian-les-Bains, France

ARTICLE INFO

Keywords:
Water resource
Volcanic Island
Tropical climate
High resolution rainfall product
Climatic reanalysis
Remote sensing

ABSTRACT

Study region: Water resource management relies fundamentally on our ability to monitor climate forcing variability, especially in tropical mountainous environment where the temporal and spatial variability of rainfall strongly controls the dynamics of the water resource. In West Java Island, rainfall temporal and spatial distribution significantly varies in function of regional climatology and volcanoes morphology while accessibility issues and the complexity of climatic phenomena notably are limitations for reliable rainfall ground instrumentation.
Study focus: Here, we assess the ability of climate reanalyses (CHELSA and TerraClimate) and satellite products (CHIRPS) in capturing rainfall high resolution spatial variability. The accuracy of rainfall amounts, variability and dynamics of each global product is estimated using the three component of Kling-Gupta efficiency score. As direct statistical comparison is influenced by resolution issues, our approach is completed by a process-based one. The spatial and orographic rainfall patterns of the global products are analyzed according to known climatic phenomena.
Hydrological Insights: It appears that, TerraClimate provides the most accurate and stable estimation for temporal monitoring. CHIRPS shows consistent rainfall patterns with atmospheric circulation and volcanoes morphology but overestimates overall rainfall amounts. This study presents a methodology for assessing global climatic products over poorly instrumented areas. The results demonstrate that high resolution global products are somewhat interesting for water resources management. However, several temporal and spatial biases still limit their integration for operational purposes.

1. Introduction

In volcanic islands, water demand (for irrigation, drinking water, industry, etc.) is more and more satisfied by groundwater, as surface water may not be available during the dry season, and may also be of poor quality (Charlier et al., 2011; Lachassagne et al., 2014; Vittecoq et al., 2019). On such geological settings, volcanic aquifers are usually considered as highly productive which means

* Corresponding author.
E-mail address: marc.dumont@sorbonne-universite.fr (M. Dumont).

https://doi.org/10.1016/j.ejrh.2022.101037
Received 2 August 2021; Received in revised form 19 December 2021; Accepted 9 February 2022

that the volcanic rocks have a high hydraulic conductivity, that allows a high discharge to be pumped, often more than 100 m^3/h per borewell (Charlier et al., 2011; Lachassagne et al., 2014; Vittecoq et al., 2019). Due to its utmost importance, such groundwater resource must be sustainably managed, which means that the groundwater abstraction should not, on average, exceed the average

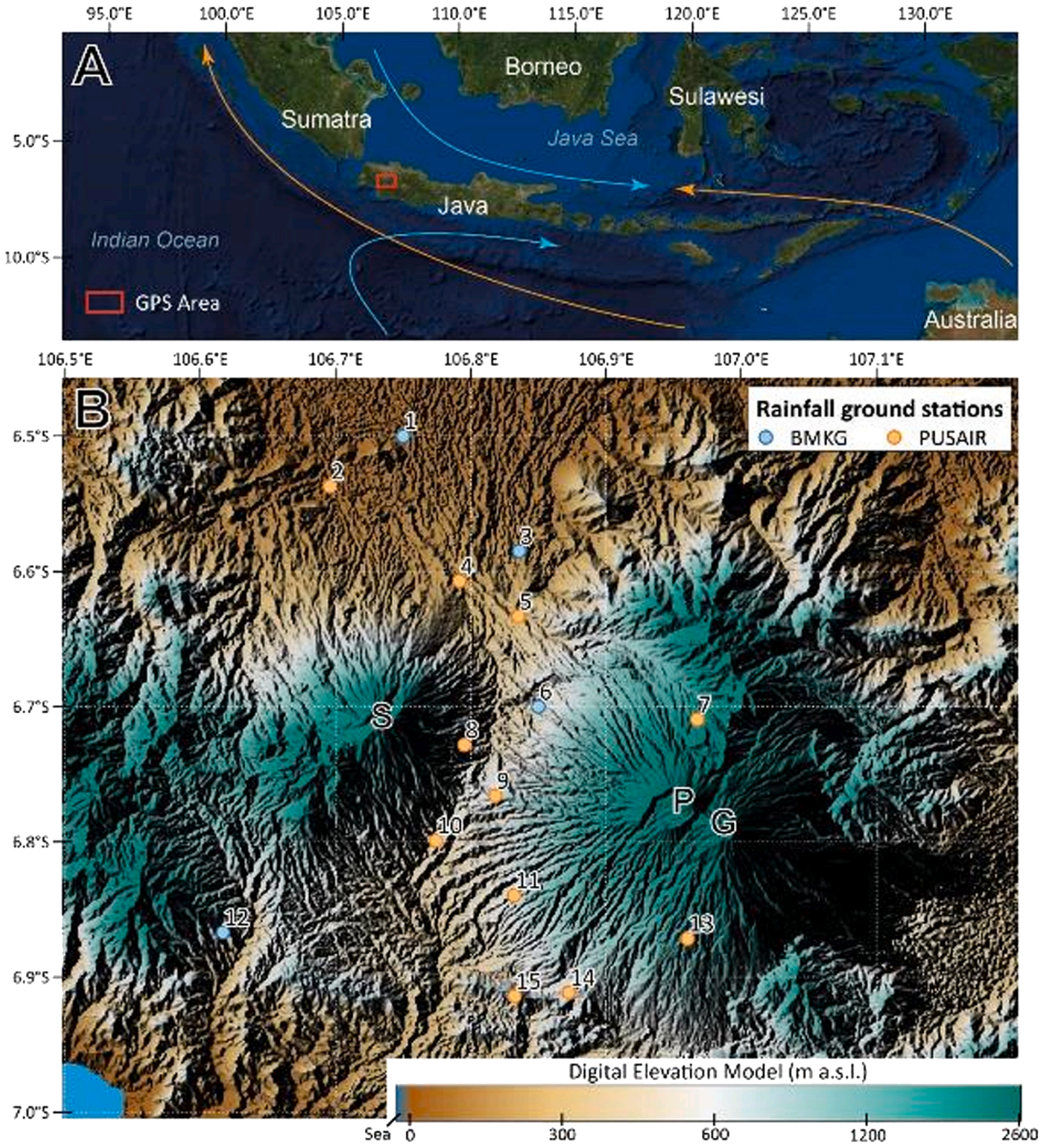

Fig. 1. (A) Map of Java island and surrounding islands. The study area, Gede, Pangrango and Salak (GPS) volcanoes, is delineated in red. The blue and orange arrows correspond to major wind directions during wet and dry seasons, respectively. These main wind direction have been estimated from wind monthly regimes defined using u and v component of ERA5 monthly averaged wind data on single levels from 1979 to present (Hersbach et al., 2020). The wind regime maps are presented in supplementary material A. (B) Study area with the three volcanoes: S for Salak, P for Pangrango and G for Gede. The 15 ground rain gauges are located with blue and orange dots for BMKG and PUSAIR meteorological services, respectively. The digital elevation model is extracted from the Shuttle Radar Topography Mission (SRTM) dataset with a 90-m lateral resolution. Coordinates are given in WGS84 - World Geodetic System 1984 - EPSG 4326.(For interpretation of the references to colour in this figure, the reader is referred to the web version of this article.)

recharge rate of the considered aquifer. Thus, groundwater resource sustainability is highly dependent on the variability of climatic forcing. In Indonesia, especially in Java Island, the exponential raise of water demand for agriculture, industry, and domestic water use gradually increases the stress on the available groundwater resource. Previous studies demonstrated that aquifer recharge may occur along all the volcano slopes (Dumont et al., 2021; Toulier et al., 2019), and that aquifer recharge is thus highly dependent on the spatial and temporal patterns of rainfall and evapotranspiration. These patterns highly depend on the altitudinal climatic variability which can be very high in such a tropical humid and mountainous setting, and can hardly be characterized with sparse ground rain gauges, notably for cost and accessibility reasons.

In Indonesia, the climate is characterized by a tropical seasonality with a dry season from April to October and a wet period from November to March (Aldrian and Susanto, 2003). In addition, the climatic variability is impacted by several factors. Java Island is located nearby the equator and surrounded by the Indo-Pacific Warm Pool (IPWP) where the Hadley cell and the Walker circulations converge yielding several specific rainfall regimes over Indonesia (Aldrian and Susanto, 2003). The first climatic driver is induced by the Asian-Australian monsoon affecting the Indonesian climate with circulations originating from the Northwest during the wet season (December to February), while Southwest winds occur during the dry season (June to July; Fig. 1; Aldrian and Susanto, 2003; As-syakur et al., 2013; Chang et al., 2005). The second climatic driver comes from steep topography of young volcanoes which impacts the circulation of the hot and humid air masses generated by the IPWP leading to strong spatial and temporal rainfall variability (Houze, 2012; Qian, 2008; Sobel et al., 2011). This orographic influence varies according to the seasons and the evolution of the inversion layer creating strong rainfall heterogeneity between windward, leeward and even on the same slope (Réchou et al., 2019). The third climatic driver controlling the climatic variability of Java Island is composed by El Niño-Southern Oscillation (ENSO) and the Indian Ocean Dipole (IOD) (As-syakur et al., 2014; Lestari et al., 2018; Qian et al., 2010). These two interconnected regional phenomena create high interannual climatic variability over Indonesia impacting both monsoon and orographic processes.

In hydrogeological studies with a perspective of water resource management, the characterization of such variability is usually addressed with the help of dense ground rain gauge networks (Charlier et al., 2011; Toulier et al., 2019; Vittecoq et al., 2020). However, recent andesitic volcanoes are characterized by steep slopes limiting access at medium to high elevation. Thus rain gauge monitoring is generally concentrated in the valleys between the volcanoes, limiting the understanding of orographic effects induced by volcano slopes and dominant wind orientations (Satgé et al., 2019). In order to complete or replace ground rain gauge data, global products are targeted to provide spatially and temporally continuous climatic dataset (Sun et al., 2018). These datasets are generally characterized by large grids with sizes ranging from 0.5° to 2.5°. Such resolutions are not suited to monitor orographic effects on volcano slopes. Nevertheless, recent development of high resolution downscaling methodologies is opening up new opportunities at local scale (Fick and Hijmans, 2017; Hersbach et al., 2020).

Global products are generally derived from the interpolation of ground rain gauges data (Becker et al., 2013; Dee et al., 2011), or from the processing of remote sensing data (Huffman et al., 2007). Both approaches lead to uncertainties in the estimation of rainfall volumes and variability. Climatic reanalysis relies on ground data availability and the accuracy of interpolation methods. Satellite-based rainfall products are indirect measurements (microwaves or infrared) of low earth orbital. The rainfall monitoring of short precipitation events is inaccurate due to the sampling rates of the satellites. In mountainous settings, the presence of warm clouds could create similar signals as rainy clouds, hence biasing the satellite estimates (Satgé et al., 2019).

In order to assess the validity of global products, several methodologies have been developed. The first one consists in direct comparisons of ground rain gauge data with global products. This approach faces several limits such as the quality of ground monitoring and the difference of resolution. The point-scale monitoring of rain gauge station may not represent areal precipitation captured by global products. Tang et al. (2018) demonstrated that the smaller the number of stations, the more the comparison will underestimate the quality of the overall products. This resolution bias can be solved by using ground radar signals that monitor rainfall over large areas in a distributed way (Satgé et al., 2019). Nevertheless, the estimation of rainfall from ground radar is complex and it is biased in mountainous areas (Zeng et al., 2018). The second approach consists in analyzing the sensitivity of hydrological modelling to global products (Maggioni and Massari, 2018; Satgé et al., 2019). Several studies analyzed global products performance over mountainous area in Andean Plateau (Elgamal et al., 2017; Satgé et al., 2019), African Eastern Plateau (Dinku et al., 2008; Gebremicael et al., 2017; Goshime et al., 2019), Tibetan Plateau (Alazzy et al., 2017; Shrestha et al., 2017), and even recently over tropical islands (Bathelemy et al., In review). Nevertheless, these studies evaluated global products at regional scales, from few to dozen earth degrees, which does not provide specific guidance for the management of local groundwater resources at a scale from 10 to a few 1000 km^2.

Our study takes part of a multidisciplinary project for groundwater management on headwater catchment of Jakarta on Java Island. The studied area of about 4000 km^2 includes three Indonesian stratovolcanoes (Fig. 1.B): Salak (2200 m a.s.l.), Gede (2958 m a.s.l.), and Pangrango (3019 m a.s.l.). Aligned from North to South, a large valley separates the Salak from the Gede-Pangrango that are embedded together forming a single more massive edifice. These three volcanoes are a portion of the Indonesian volcanic arc extending from Sumatra to East Java, and to the eastern chain of islands including Bali, Lombok and Flores. Orographic effects induced by the combination of the volcanic chain and regional winds direction, might differ spatially and evolve during the year (Fig. 1.A). According to the maps of monthly wind (see supplementary material A), the climate of the northern slopes should be mainly impacted by atmospheric circulations from Asia, while the southern part might be more impacted by Australian climatic conditions. Finally, climatic conditions in the valley might be largely influenced by local processes induced by topographic irregularities.

In order to understand rainfall patterns in a such limited area impacted by local climatic phenomenon, we compare scarce ground rain gauge data with three global products: CHELSA, a 1-km grid length product from ERA-Interim reanalysis downscaling; TERRA, a 4-km grid length dataset from WorldClim and CRU reanalysis downscaling; and CHIRPS, a 5-km lateral resolution downscaling of TMPA 3B42 remote sensing dataset (Abatzoglou et al., 2018; Funk et al., 2015; Karger et al., 2017). The temporal resolution of the global products is relatively coarse (up to one month) but still interesting for water resource management applications. The first

objective of this study is to estimate the accuracy of these three global products over tropical mountainous areas using scarce ground rain gauge data. Given that there is no rainfall amount monitoring derived from ground radar data available and that river discharge monitoring dataset in the sector are too short and incomplete, the quantitative evaluation of global product relies only on ground gauge data. As such comparison is biased by resolution issue, the second objective is to provide a process-based analysis of spatial rainfall patterns and orographic effects. This analysis relies on the comparison of global and ground rainfall patterns with local spatial trends and orographic effects from previous studies in tropical Island. Finally, these results will help to evaluate whether global products are accurate enough to be used for the sustainable management of groundwater resources. The combination of quantitative and qualitative analyses will provide an overview of the strengths and limits of ground and global monitoring products to quantify rainfall over tropical volcanoes for operational groundwater resource management.

2. Material and method

2.1. Ground rain gauges

In the area, the daily monitoring dataset from 34 ground rain gauge was collected. A quality check was performed for each station using cumulative and double-mass curves. The purpose of this procedure is to ensure that each station temporal dynamics is consistent with neighboring gauges as well as with climatological knowledge. After this quality check, 15 stations from two providers have been conserved: 4 stations from BMKG[1] and 11 from PUSAIR[2] (Fig. 1.B; Table 1). In order to compare these data to global products, monthly total rainfall have been calculated when less than 10% of the month data is missing. These stations are mainly located in the valleys at low elevation (between 133 and 1134 m, average 510 m). In addition, the spatial distribution of ground stations is highly heterogeneous with a concentration in the valley between Mt. Salak and Mt. Pangrango, as well as in the northern slope of Mt. Salak and southern part of Mt. Gede (Fig. 1.B).

2.2. Global products

In this study, we do not intend to provide an exhaustive overview of all available products. The objective is to provide a detailed assessment of the strengths and weaknesses of the different high resolution global products in such tropical orographic settings. The global rainfall products have been selected according to three requirements: (i) a lateral resolution below 10 km to analyze spatial variability, (ii) a time series long enough to analyze temporal variability, and (iii) several reanalysis and remote sensing protocols to discuss the relative merits of each method. Three global products have been selected (Table 2): CHELSA (Climatologies at High resolution for the Earth's Land Surface Areas), TERRA (TerraClimate), and CHIRPS (Climate Hazards Group InfraRed Precipitation with Station data).

2.2.1. CHELSA – Climatologies at High resolution for the Earth's Land Surface Areas

CHELSA climate reanalysis at monthly basis originates from the downscaling of ERA-Interim climatic reanalysis to a 1-km resolution (Dee et al., 2011; Karger et al., 2017).[3] In order to improve precipitation resolution and accuracy, the downscaling algorithm incorporates orographic predictors including wind fields, valley exposition, and boundary layer height, with a subsequent bias correction. The resulting data consist of monthly temperature and precipitation time series over the 1979–2018 time period. This dataset was compared with other standard gridded products and stations data from the Global Historical Climate Network (GHCN) by Karger et al. (2017) who showed that CHELSA product provides a better accuracy of rainfall range predictions compared to other global climate modelling products such as CRU and ERA-Interim.

2.2.2. TERRA – TerraClimate

TERRA is a 4-km gridded dataset at monthly time step that combines several climate reanalyses (Abatzoglou et al., 2018)[4]: WorldClim v1.4 and v2 (Fick and Hijmans, 2017; Hijmans et al., 2005), CRU Ts4.0 (Harris et al., 2020), and JRA-55 (Kobayashi et al., 2015). The compilation of the original data is done in four steps. In the first step, high resolution monthly climate averages are derived from WorldClim v2 integrating average mean temperature, vapor pressure, precipitation, solar radiation at the surface, and wind speed. As WorldClim v2 presents several biases in diurnal temperature range, WorldClim v1.4 is used to calculate maximum and minimum temperature during the second step. The third step consists in creating climate anomaly time series with lower spatial resolution products, namely CRU Ts4.0 and JRA-55. Then, TERRA rainfall dataset is created by superimposing monthly climate anomalies from step 3 to monthly climate normal from steps 1 and 2. This is carried out using a climatologically aided interpolation consisting of a simple spatial downscaling with bilinear interpolation of temporal anomalies from a higher-temporal, lower-spatial resolution dataset to a lower-temporal, higher-spatial resolution dataset (Mosier et al., 2014; Willmott and Robeson, 1995).

[1] Badan Meteorologi, Klimatologi, dan Geofisika - www.bmkg.go.id
[2] Pusat Penelitan Dan Pengenbangan Sumber Daya Air - http://www.pusair-pu.go.id/
[3] https://envicloud.wsl.ch/#/?prefix=chelsa%2Fchelsa_V2%2FGLOBAL%2Fmonthly%2Fpr%2F.
[4] http://thredds.northwestknowledge.net:8080/thredds/terraclimate_aggregated.html?dataset=agg_terraclimate_ppt_1958_CurrentYear_GLOBE.

Table 1
List of rainfall ground stations. Data availability is expressed in number of months over the period January 2001 – December 2018 (216 months). Coordinates are given in WGS84 - World Geodetic System 1984 - EPSG 4326.

Id	Provider	Name	Longitude (°)	Latitude (°)	Elevation (m)	Data availability	
						(months)	(%)
1	BMKG	Staklim-Bogor	106.75000	-6.50000	133	135 / 216	62.5%
2	PUSAIR	Cihideung-Udik	106.69583	-6.53722	141	180 / 216	83.3%
3	BMKG	Darmaga	106.83580	-6.58500	222	73 / 216	33.8%
4	PUSAIR	Empang	106.79167	-6.60722	258	99 / 216	45.8%
5	PUSAIR	Katulampa	106.83528	-6.63333	342	144 / 216	66.7%
6	BMKG	Stamet-Citeko	106.85000	-6.70000	492	216 / 216	100%
7	PUSAIR	Gunung-Mas	106.96750	-6.70944	1134	192 / 216	88.9%
8	PUSAIR	Pasir-Jaya	106.79528	-6.72833	517	180 / 216	83.3%
9	PUSAIR	Manggis	106.81833	-6.76583	583	48 / 216	22.2%
10	PUSAIR	Cicurug-Ciutara	106.77417	-6.79917	465	108 / 216	50%
11	PUSAIR	Sinagar	106.83194	-6.83972	581	132 / 216	61.1%
12	BMKG	KbSalak	106.61670	-6.86700	507	111 / 216	51.4%
13	PUSAIR	Cisalada	106.96028	-6.87167	944	84 / 216	38.8%
14	PUSAIR	Ciraden	106.87250	-6.91139	567	180 / 216	83.3%
15	PUSAIR	Cibadak-Cisekarwangi	106.83250	-6.91417	630	108 / 216	50%

Table 2
Presentation of the three global products used in this study.

Name	Version	Type	Initial products	Spatial resolution	Time period
CHELSA[3]	V 2.1	Climatic reanalysis	ERA-Interim	1/125°	1979 – 2018
TERRA[4]	V 1.0	Climatic reanalysis	WorldClim v1.4 CRU Ts4.0	1/24°	1958 – 2020
CHIRPS[5]	V 2.0	Remote sensing	TMPA 2B31	1/20°	1981–2020

2.2.3. *CHIRPS – climate hazards group infrared precipitation with station data*

CHIRPS (Funk et al., 2015)[5] comprises gauge stations analysis, infrared Cold Cloud Duration (CCD) observations and bias correction in a 3-step algorithm. The first step is the creation of a monthly precipitation climatology model, CHPclim, that incorporates FAO (Food and Agriculture Organization) and GHCN (Global Historical Climatology Network) station monthly averages, typical physiographic indicators (elevation, latitude, and longitude) and monthly long-term mean rainfall from four satellite products: TMPA 2B31 (Huffman et al., 2007), CMORPH (Joyce et al., 2004), Global infrared data (Janowiak et al., 2001), and MODIS (Wan, 2008). As a result, CHPclim produces monthly, pentadal (10 days), and daily climate averages. The second part of the computation consists in using central composite design CCD regression slopes to estimate rainfall from satellite imagery and compare it with CHPclim climate normal. The third step is the combination of extensive ground gauge datasets and CHIRP precipitation to compile CHIRPS estimates of monthly precipitation monitoring. Only one of the six stations used to correct for CHIRPS in West Java is located in a mountainous area.

2.3. *Objective 1: Temporal ground – global products quantitative evaluation*

The first objective of the analysis consists of providing a quantitative evaluation of the three global products by means of statistical metrics. We compare global products with ground rain gauge data from its corresponding cell (Fig. 2). This analysis aims to assess the differences between ground-based and gridded datasets in terms of (1) precipitation amounts, (2) seasonal variability, and (3) dynamic consistency. To do so, we present three statistical criteria where ground rain gauge are considered as reference named R, and evaluated global products are named E. These criteria are components of the Kling-Gupta efficiency (KGE) criterion (Gupta et al., 2009) in order to analyze separately volume, variability and dynamic bias rather analyzing an overall score. Taylor diagrams that use Root Main Square (RMS) criterion are presented in the Supplementary material B.

First, mean and standard deviation (STD) ratios, named β and α respectively, are calculated to quantify differences in terms of volumes and variability between the references and evaluated monthly data:

$$\mu_E = \frac{1}{N} \sum_{i=1}^{N} E_i \quad \sigma_E = \sqrt{\frac{1}{N-1} \sum_{i=1}^{N} |E_i - \mu_E|^2}$$

$$\beta = \frac{\mu_E}{\mu_R} \qquad \alpha = \frac{\sigma_E}{\sigma_R}$$

[5] https://data.chc.ucsb.edu/products/CHIRPS-2.0/global_monthly/.

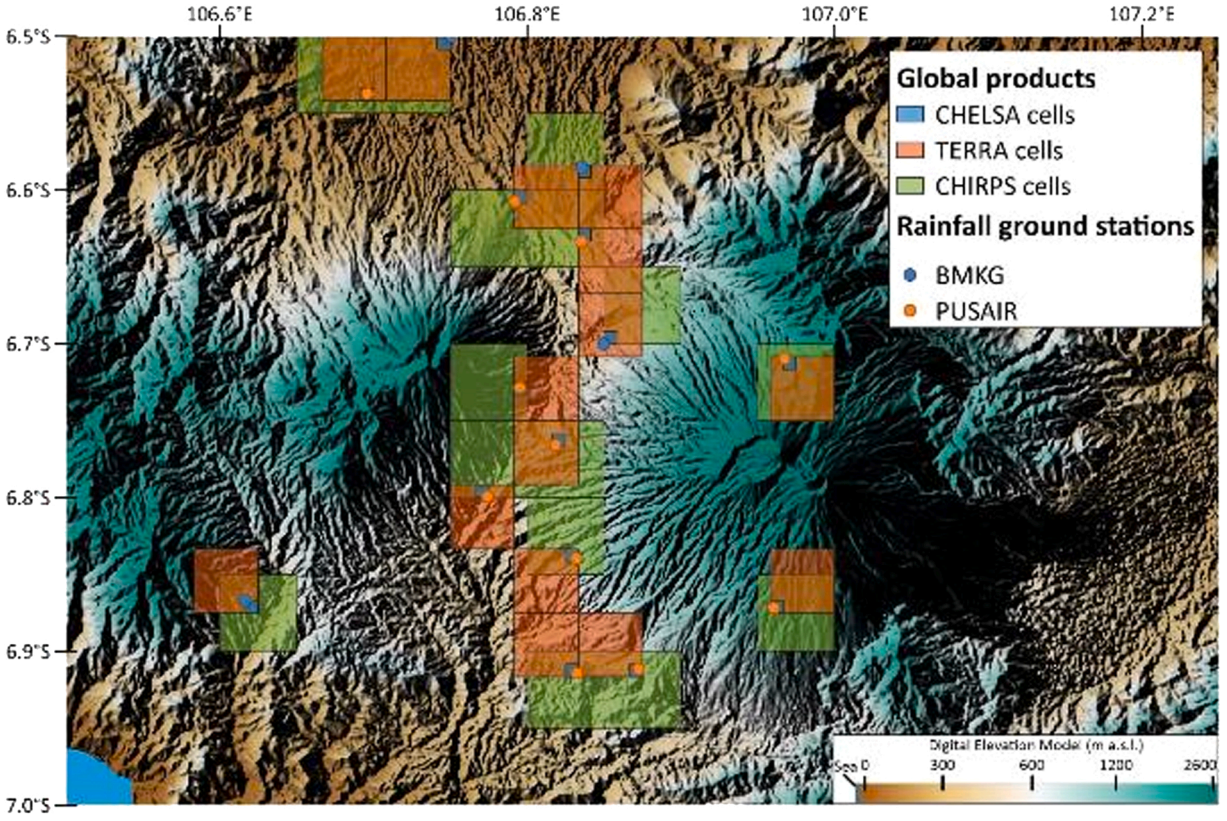

Fig. 2. Location of all ground stations and corresponding cells of global products CHELSA, CHIRPS and TERRA.

with μ the mean and σ the standard deviation of the monthly data calculated over the period N. In this case, β assesses the volumes bias between the two time series, whereas α estimates the variance bias. For both criteria, the ideal value is then 1, indicating a perfect fit between rain gauge data and global product in terms of mean amounts and standard deviation.

Second, the Pearson correlation coefficient (CC) evaluates the error in dynamics and timing between the reference and evaluated time series. The ideal value for CC is 1. The CC calculation is combined with an estimation of its p-value in order to assess the CC validity.

$$CC = \frac{1}{N-1}\sum_{i=1}^{N}\left(\frac{E_i-\mu_E}{\sigma_E}\right)\left(\frac{R_i-\mu_R}{\sigma_R}\right)$$

These three criteria are first calculated for the three global products over the entire time series (N *range from* 48 *to* 216 in function of

Table 3
Annual rainfall, in meter, between 2001 and 2018 for the fifteen ground rain gauge.

Id	01	02	03	04	05	06	07	08	09	10	11	12	13	14	15	16	17	18
1								3.5	2.0	2.6	1.7	3.0	2.5	4.2				
2			3.2	2.7	3.5	2.1	3.9	3.7	3.5	4.2	3.0		4.2	4.7	2.8	2.1	4.0	2.6
3								4.0	3.5	4.0	2.9	3.6						
4			2.8	3.9	4.3	2.5	2.8	3.9	3.5	5.4	3.0							
5			2.6	4.8	4.5	2.9	3.4	4.2	3.8	5.2	2.8	2.6	3.1	3.5				
6	3.7	3.0	2.8	2.8	3.1	2.6	3.5	3.2	3.3	3.6	2.4	2.7	2.5	2.5	0.0	1.4	2.9	2.1
7			1.6	2.8	3.7	2.3	2.7	3.5	4.0	4.6	2.5	2.3	4.1	3.6	2.8	2.5	3.6	3.4
8		3.4	3.1	4.4	3.3	2.7	3.2	3.7	4.4	6.1	2.7	3.8	5.2	3.0	2.6			
9		3.2	3.1	2.7	2.8	2.4												
10										4.5	2.8	2.6	3.1	3.5	2.3	4.1	3.1	2.9
11					1.9	1.9	2.2	2.9	2.2				2.9	2.6	1.9	3.5	2.4	2.1
12										3.0	2.3	2.8	1.8	1.9	1.8	2.2	2.2	2.2
13		2.7		2.5	2.4	1.8	2.6	3.0	2.7									
14				2.1	2.9	2.2	2.3	2.7	2.6	3.9	2.3	2.3	2.5	2.1	1.9	3.0	2.3	2.0
15										3.7	1.3	2.4	2.2	2.4	2.2	3.2	2.6	2.3

the ground rain gauge). Then, they are averaged for each station, giving 15 scores for each global product, one for each station. This first standard approach aims at providing an overview of the accuracy of global product relative to ground stations. Nevertheless, global product accuracy could vary temporally requiring to work on different temporal scales (Satgé et al., 2019). Water management at watershed scale needs accurate monitoring of both seasonal and interannual variability of the rainfall in order to set up short- and long-term sustainable management. In order to evaluate interannual bias, statistical criteria are thus calculated for each year only ($N = 12$). For this step, only complete years of ground rain gauge time series are used (Table 3). The 15 scores for each station are then presented using a box plot. Finally, a third calculation is made for each month separately (i.e., January, February, etc., $N = 18$). This allows the evaluation of global products ability to capture the seasonality over the entire period. All the statistical results are showed in the Supplementary material D and E.

2.4. Objective 2: Spatial analysis of the consistency of rainfall products in capturing orographic effects

The second objective consists in analyzing the spatial distribution of ground-based and global rainfall products in order to examine their relative consistency with regards to orographic effects. Given the specific context of the three studied tropical volcanoes, this investigation is of high interest by evaluating the products ability to describe orographic effects at kilometric scale.

Indeed, the variability of orographic phenomena is a function of the type of atmospheric circulation, season, organization of slopes as well as the altitude of the inversion layer (Houze, 2012). The orographic gradient is regularly used to understand these phenomena and approximate the evolution of rainfall as a function of altitude. Körner (2007) defined different altitudinal gradients according to the climates defined by the latitude of the area. As Java Island is located around 6°S latitude, the gradient should correspond to the equatorial pattern (0–10° latitude) characterized by a rainfall decrease as a function of altitude, accentuated above 1500 m altitude (Körner, 2007). However, Toulier et al. (2019) rather found a sub-tropical pattern (like the 10–30° latitude one) on the northern slope of the Bromo-Tengger (East of Java Island). In their study, a network of ground stations showed a rainfall increase with the elevation up to 1000–1400 m a.s.l., above which the annual rainfall decreased up to the 3000 m a.s.l. at the summit. Finally, recent studies showed the strong seasonal variability of this orographic gradient. In the Indian Ocean, the influence of the position of the Intertropical Convergence Zone on La Réunion Island's local climate as well as on atmospheric circulations (e.g. trade winds or cyclones) induces a strong temporal variability of the orographic gradients (Réchou et al., 2019).

In this study, orographic effects were analyzed on homogenous geo-climatic areas defined according to volcanoes morphology and monthly wind regional and local atmospheric circulations (see supplementary material C). As presented by blue and orange arrows in

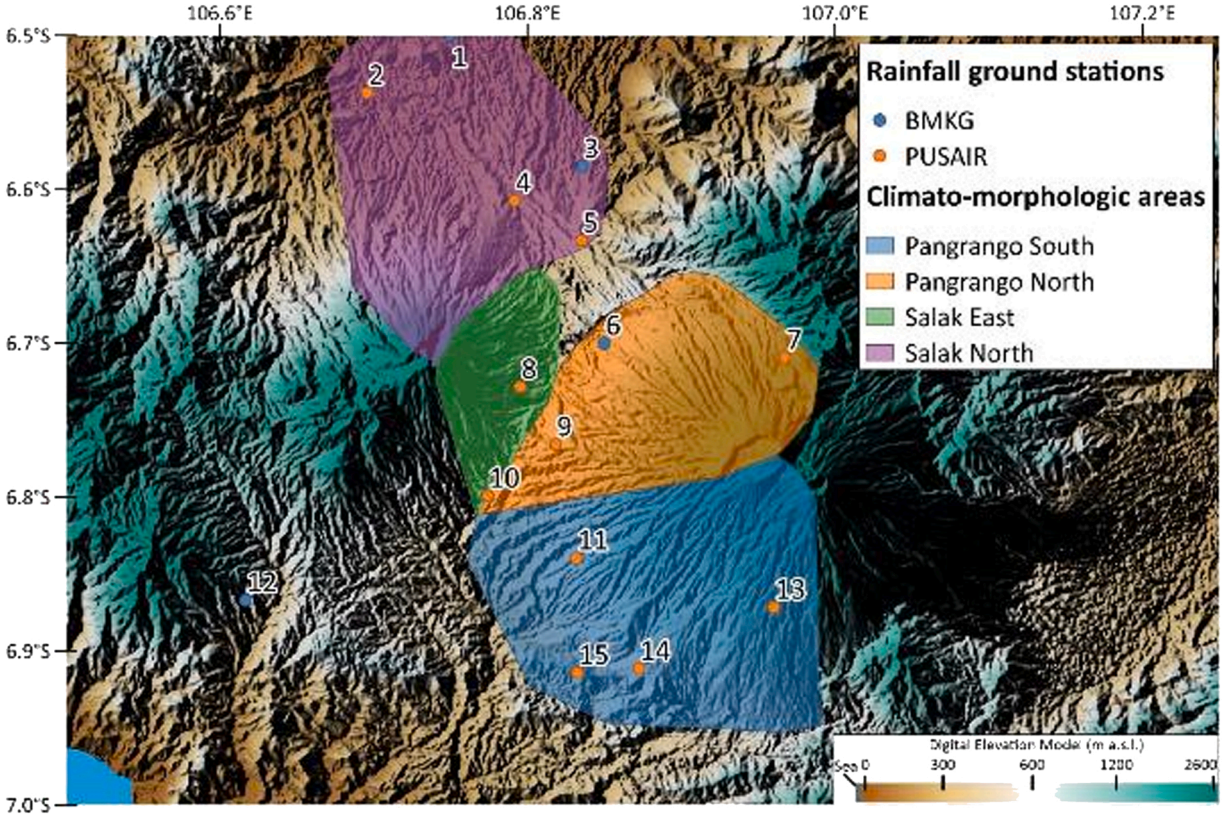

Fig. 3. Definition of the four geo-climatic areas on the study area.

Fig. 1.A, atmospheric circulations are mainly influenced by the Asian-Australian monsoon. During the wet season, the Australian monsoon induces atmospheric circulations from north-west to south-east over the study site (blue arrows). Dominant winds present inverse directions during the dry season (orange arrows) with the Asian monsoon (Aldrian and Susanto, 2003). Consequently, four geo-climatic areas were defined on the studied area (Fig. 3). Each areas are defined in order to gather at least 2 ground rain gauges in distinct geomorphological region:

1. Salak North (stations 1–5): directly facing Java Sea, rainfall regimes and orographic effects on this slope are assumed to be directly controlled by northern atmospheric circulations during the Australian Monsoon.
2. Salak East (stations 8 and 10): oriented towards the east in the valley between Salak and Pangrango, this slope should be affected by both north and south atmospheric circulations as well as local orographic effects.
3. Pangrango North (stations 6, 7 and 9): this slope of Pangrango is surrounded by the Salak volcano at the West and by an old volcano at the North. Mainly impacted by northern conditions, rainfall regimes should also be impacted by local orographic effects.
4. Pangrango South (stations 11, 13–15): This slope in the southern part of the study faces the Indian Ocean. Rainfall regime in this area is assumed to be directly impsacted by southern climatic conditions.

In these conditions, station number 12 was not attributed to any region. Two analyses have been carried out for each zone. The average rainfall patterns of the three climate reanalyses were compared according to the four main seasons: the wet season (December to February - DJF), the transition to the dry season (March to May - MAM), the dry season (June to August - JJA), and the transition to the wet season (September to November - SON). Then, the altitudinal rainfall gradients were analyzed.

3. Results

3.1. Objective 1: Temporal ground – global products quantitative evaluation

In order to examine the overall accuracy of the three global products, we conducted a straightforward statistical comparison between global products and ground rainfall data. To do so, statistical criteria for the three global products are calculated in relation to each station and their distributions are shown in Fig. 4. Since ground rain gauges are distributed across the different geo-climatic areas defined previously, the variability of statistical scores, i.e. the box height, would reflect the relative ability of global products to capture the spatial variability of ground-based precipitation amount, temporal variability, and dynamics. In order to understand spatial variability, a map of each criterion is presented below in Fig. 5).

This first broad analysis provides an interesting overall evaluation. The ratio of means β highlights a good consistency for TERRA (median scores: 1.01), while CHELSA and CHIRPS generally overestimate rainfall amounts (median score: 1.37 and 1.21). The distribution of the ratio of means is rather tight for TERRA and CHIRPS (interquartile range: 0.98–1.12 and 1.13–1.33, respectively), which is consistent with the spatial distribution of β (Fig. 5). In comparison CHELSA is characterized by a wider distributions (interquartile range: 1.04–1.65; Fig. 4.A). The spatial distribution of the ratio of means β demonstrate a rainfall overestimation in the southern part -for each global products (Fig. 5). In contrast, rainfall amounts estimation is more accurate in the northern and center

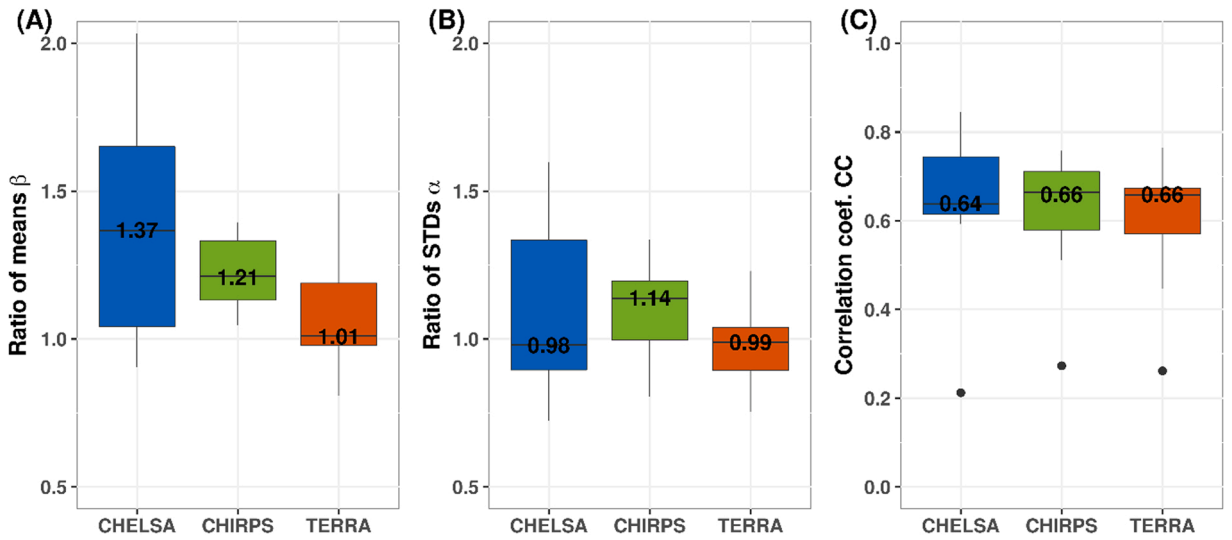

Fig. 4. Distributions of (A) Ratio of means β, (B) ratio of STDs α, and (C) Correlation coefficient CC. For all global products, the box plots are constructed with the value of the 15 global stations from Fig. 2 estimated over the entire time period. The boxes are delimited by the first and third quartiles. Values indicate the median of each distribution. Statistical tests suggest that *100*% of the CC values were significant for CHELSA, as well as *87*% for CHIRPS and TERRA. All the statistical results for each stations are presented in supplementary material D tables.

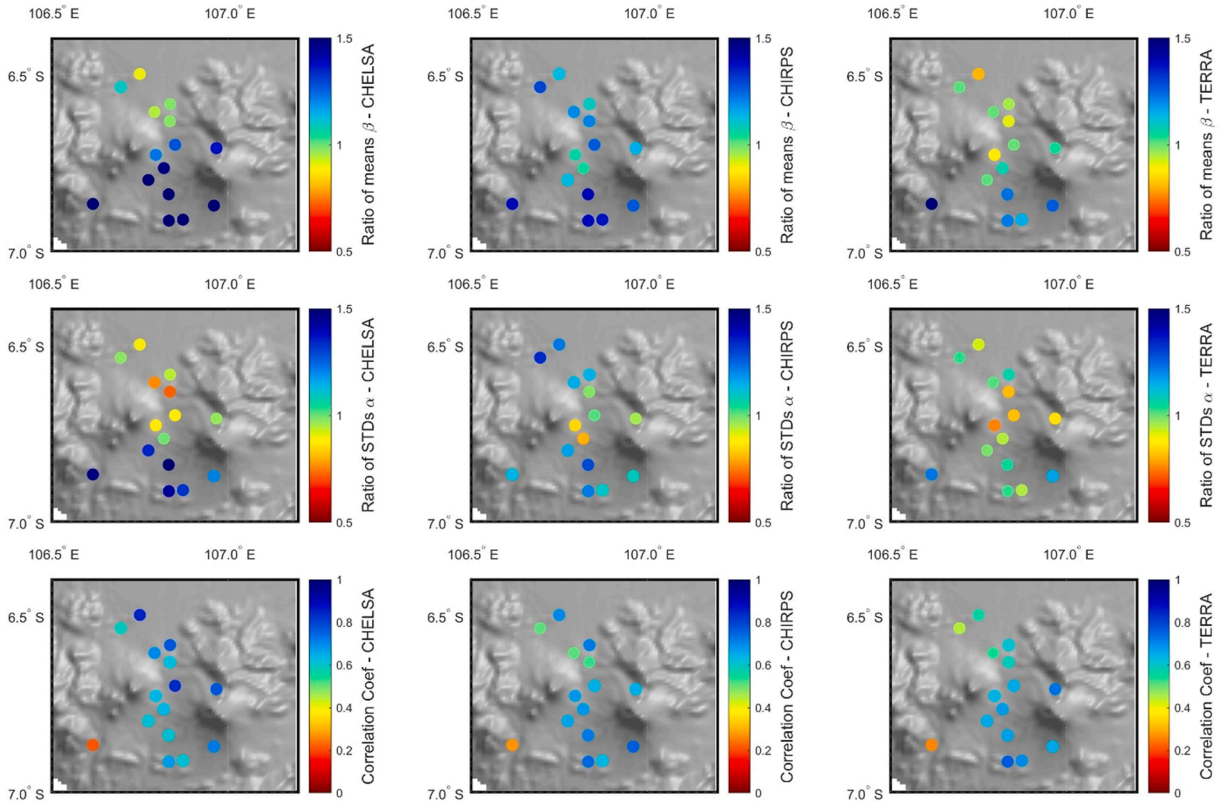

Fig. 5. Spatial ratio of means β (1st line), ratio of STDs α (2nd line), and Correlation coefficient CC (3rd line) between global rainfall products and ground rain gauges. CHELSA results are presented in the left column, CHIRPS in the center and TERRA in the right column.

part. The average variability of CHELSA and TERRA product are closed to the ground dataset (median α: 0.98 and 0.99), while CHIRPS is slightly higher (median values of α 1.14). The wider distribution of α ratios highlights the low consistency of CHELSA in estimating the spread of ground rain gauge data (interquartile range: 0.9–1.33). CHELSA underestimated the rainfall variability in the northern part of the site while it is overestimated in the south. TERRA and CHIRPS ratio of STDs are more consistent (interquartile ranges: 0.89–1.04 and 1–1.2 respectively; Fig. 4.B). Their spatial distribution is more homogeneous, with a slight STD underestimation in the valley and an STD overestimation in the northern and southern rain gauges (Fig. 5). The Pearson correlation coefficients CC of all global products appear consistent with ground rain gauge, with median values between 0.6 and 0.7 (Fig. 4.C). For each products, the CC variability in both the box plot and maps is relatively tight highlighting that global products accurately caught of the rainfall dynamics.

As monthly criteria are estimated (at this stage) over the whole time series, this calculation does not allow to analyze the temporal component of the analysis, and mixes it with spatial variability. In order to evaluate the interannual bias of the products, Fig. 6 presents the scores calculated and averaged over 12 months for each year. Fig. 6.A shows the median annual average rainfall amount in order to evaluate global product in wet years (above the median annual rainfall amount, 2008–2010 and 2013–2014) and drier ones (below the median annual rainfall amount, 2006–2007, 2011–2012 and 2015). In Fig. 6.B to D, ratio of means, STDs and CC provide information on rainfall amount bias, the seasonality contrast, and the product ability to represent the transition between seasons respectively.

The ratios of means and STDs of the CHELSA product, available up to 2018, are characterized by a wide dispersity highlighting the product limitations to reproduce the spatial variability of rainfall. CHELSA overestimates rainfall amounts most of the time especially during the last years. The median β becomes closer to 1 2008–2010. CHELSA rainfall variability varies around 1 until 2013 where it increases until 2018 demonstrating an overestimation of seasonal variability. Concerning the dynamic, the interquartiles of CHELSA's CC score are mainly above 0.5 except for years 2003, 20148, and 2016. The evolution of CHELSA's scores indicated no relationship between bias types, nor a relationship with year typology.

Concerning CHIRPS performance, the product mainly overestimates annual rainfall amounts, particularly in 2014 and 2016 (Ratio of means above 1.4). Median CHIRPS ratios of STDs mainly vary between 0.75 and 1.25. While in 2007 and 2011 this criterion stays below 1.5, it exceeds 2 in 2016. Concerning the dynamics, CC criteria is mainly above 0.6 for CHIRPS except in 2005, 2010, 2013, and 2014. It decreases even more in 2003 and 2016.

TERRA demonstrates a good consistency all over the period. Its median ratio of means β is close to 1 except for the years 2007, 2016, and 2017. The interquartiles of STD ratios are also stable between 0.75 and 1.25 except in 2007 and 2014. While the TERRA dynamics are mainly consistent with ground rain gauge (CC above 0.6), TERRA scores decrease in 2003, 2005, 2010, 2014 and 2016.

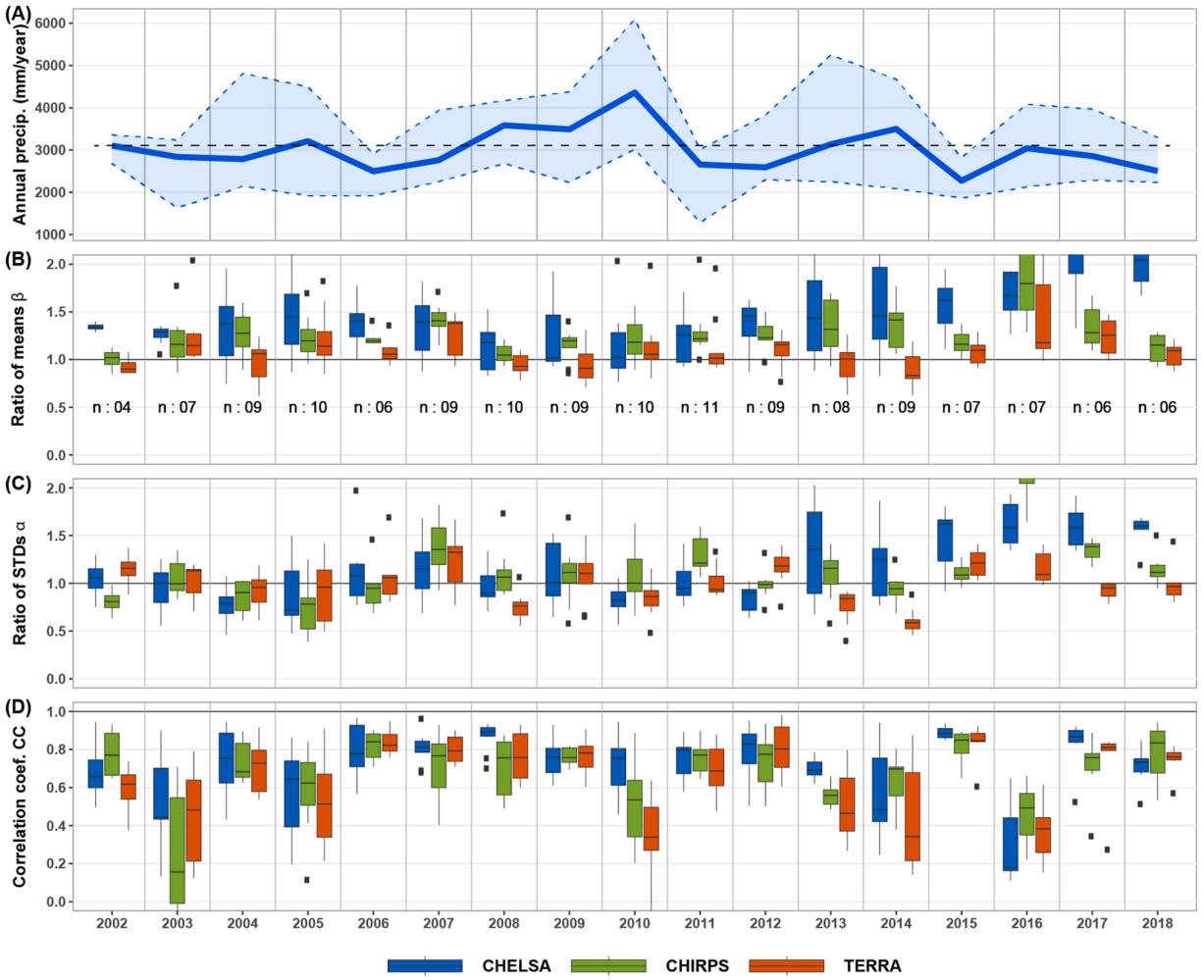

Fig. 6. (A) Median value of annual average rainfall amounts measured by ground rain gauge (in blue). The blue envelope curve highlight the min-max threshold between the 15 rain gauge monitoring, while the grey dashed line represent the annual average rainfall over the whole period. (B) Ratio of means β, (C) ratio of STDs α, and (D) CC criteria distribution for each year. The boxes are delimited by the first and third quartiles. In (B) n represent the number of ground rain gauge available. The data before 2002 were not represented because there were not enough ground rain gauge data available. Statistical tests suggest that *83*% of the CC values were significant for CHELSA, *78*% for CHIRPS and 67% for TERRA. All the annual statistical results for each stations are presented in Supplementary material D tables.(For interpretation of the references to colour in this figure, the reader is referred to the web version of this article.)

As for global calculation, CHIRPS and TERRA obtain overall better scores than CHELSA. These two global products from satellite data or climate reanalyses respectively, share some common biases: (i) errors in the dynamics in 2003, 2010 and 2013–2014; (ii) strong deviations for the three scores in 2016; (iii) and somewhat comparable correlation coefficients over the entire period. While some interannual variability in dynamics is expected, the degradation of the three criteria for all products in specific years is surprising. Finally, this interannual analysis highlights the non-linearity of global products bias limiting the possibility of debiasing them with ground rain gauge data.

The interannual analysis of global product does not provide information on their accuracy to reproduce seasonality. For this purpose, the three criteria are estimated for each month across all years (Fig. 7). It is important to remember that during the dry season, low rainfall amounts induce high bias with low volume error.

On the monthly analysis (Fig. 7A), TERRA stands out as the most accurate product in the estimation of monthly rainfall amounts (interquartile range: 1.03 – 1.18). It provide the more accurate rainfall estimation during the whole year despite a slight over-estimation in June-July and September (1.2 and 1.45, respectively). CHIRPS overestimated rainfall amounts by 10–34% (25% and 75% quartiles respectively) most of the year with a higher bias in August-September (≈ 75%), which is globally consistent with the global results (Fig. 4). CHELSA is the most inaccurate product with a large rainfall overestimation (interquartile range: 1.16 – 1.42). This seasonal analysis demonstrates that the three global products mainly overestimates rainfall amounts, especially during the transition between the dry and the wet season (August to November - Fig. 7).

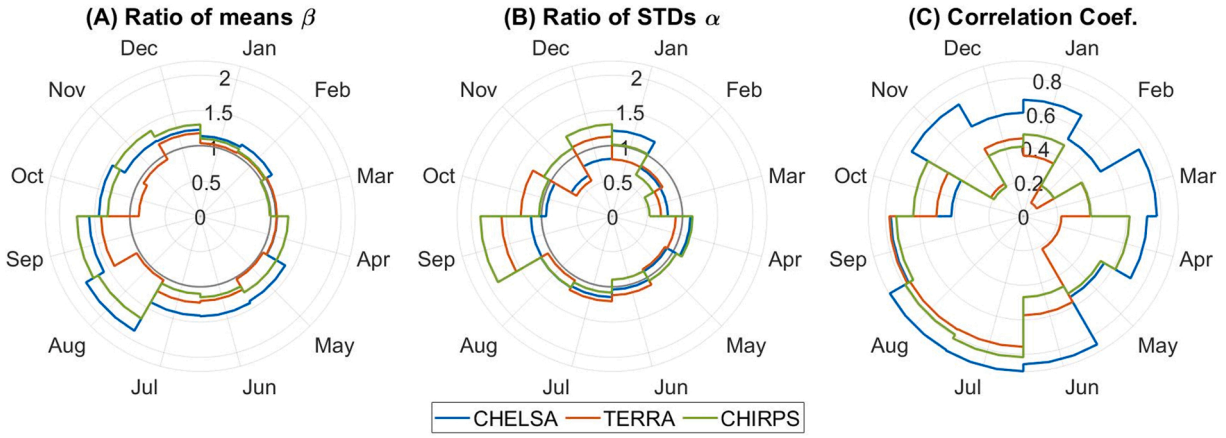

Fig. 7. Polar plot of the median value of ratio of means (A), STDs (B), and CC criteria (C) estimated for each month over the whole period. The plot represent the median value of each criterion averaged by month. It is important to remember that during the dry season, low rainfall amounts induce high bias with low volume error. Statistical tests suggest that 50% of the CC values were significant for CHELSA, *42*% for CHIRPS and 33% for TERRA. All the monthly statistical results are presented in Supplementary material E tables.

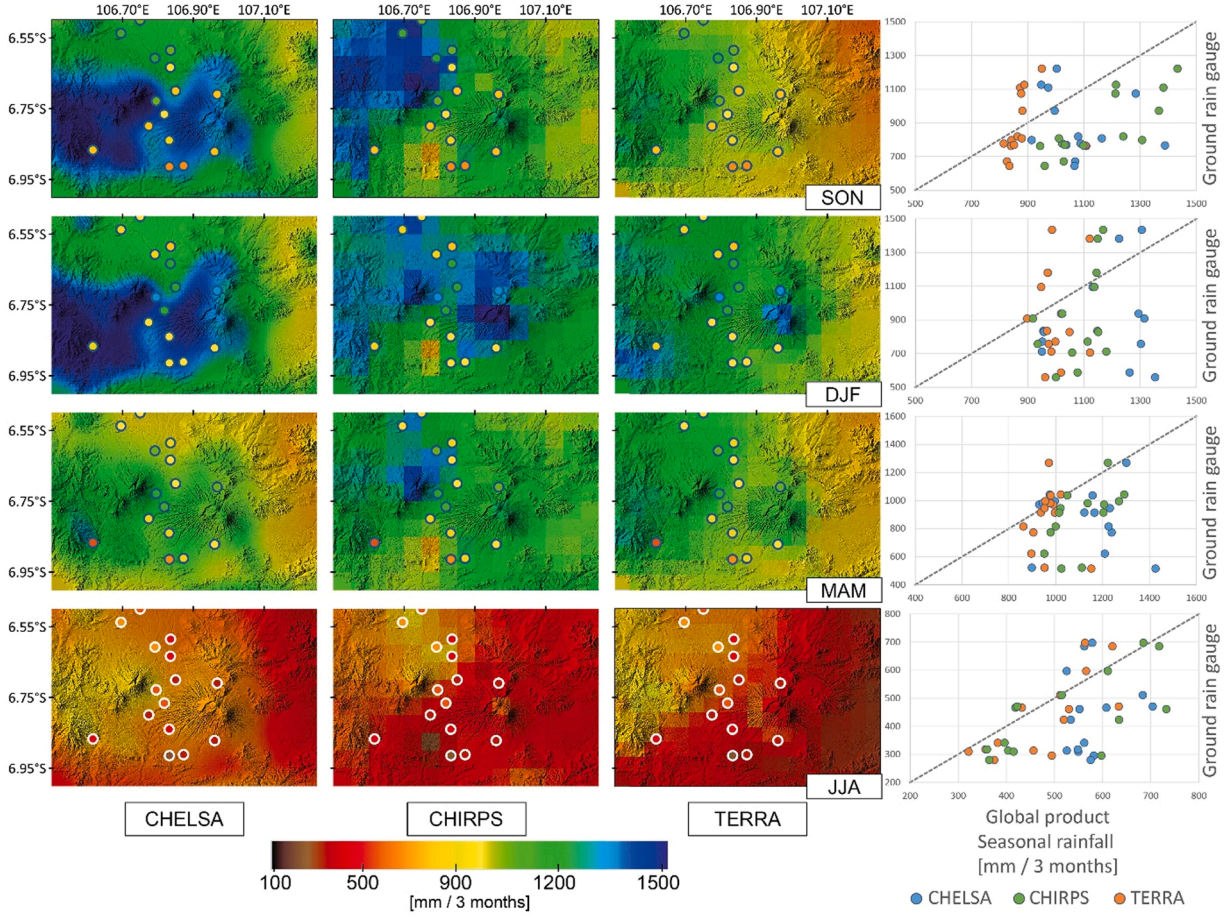

Fig. 8. Seasonal rainfall maps of CHELSA, CHIRPS, and TERRA global products average between 2008 and 2013. The hydrological year is divided in 4 seasons: September to November (SON), December to February (DJF), March to May (MAM) and June to August (JJA). The first three columns are the maps of the seasonal rainfall of each global product, where colors indicate the average rainfall volume per season for both gridded products and rain gauges. The column at the far right represents a scatter plot of the seasonal rainfall for ground rain gauge (y-axis) and the corresponding pixel of each global products (x-axis). In the scatter plots, the line 1:1 is represented by dashed gray line.

Regarding the variability (ratio of STDs - Fig. 7.B), the results are more homogeneous. TERRA and CHIRPS obtain fairly consistent results when compared one to the other (interquartile range: 0.99–1.18 and 0.82 – 1.15 respectively). However, an STD overestimation is observed on both product during September-October (from 25% to 50%). In November, February and Marchboth products importantly underestimate the variability. CHELSA obtains close scores (interquartile range: 0.81 – 1.15). CHELSA underestimate November, February and March STD but overestimate January one. It is more consistent during the year demonstrating a better capacity to catch rainfall variability during the year. This results highlights two elements: (i) annual means may be misleading for water resource management as dry season overestimation can compensate wet season underestimation, and (ii) global product tend to misestimate rainfall amounts variability during both transitions between dry and wet seasons.

Finally, concerning the rainfall dynamics (CC scores - Fig. 7.C), the three products are rather efficient during dry season (median range: 0.6–0.8), while during the wet and the transition seasons, their scores decrease (median range: 0.2–0.6). These weak scores highlight the difficulty for the three global products to capture the variation at the start/end of the wet season from one year to another. However, the decrease of p-value limits the interpretation of CC values. In supplementary material E, the statistical analysis of CC criterion highlights a low sensitivity during the wet season.

3.2. Objective 2: Spatial analysis of the consistency of rainfall products in capturing orographic effects

The statistical analysis identified some strengths and weaknesses of the global products in representing the ground rain gauge data of the study area. This analysis focused on seasonal and interannual temporally averaged spatial heterogeneities. Thus, this section first aims to understand how the different data describe the spatial distribution of rainfall according to the morphology of the three volcanoes. Second, the global products spatial trends are evaluated in order to assess if these global products may complement point ground rain gauge data to understand the spatial distribution of rainfall, especially in mountainous areas.

3.2.1. Spatial trend analysis

In order to understand seasonal patterns, the continuous gridded data from the three global products are shown in Fig. 8 along with point ground data. For each map, the average rainfall for each season from 2008 to 2013 is represented for both ground rain gauges and global products. In order to ease the comparison, a scatter plot comparing seasonal cumulative rainfall of global product with ground rain gauge is shown for each season. This period corresponds to the maximum of available ground rain gauge stations before the end of CHELSA time series (Fig. 6.B).

We define the beginning of the hydrological year at the end of the dry season from September to November (SON - Fig. 8, first row). The ground data highlight a regional rainfall gradient ranging from 1200 mm/3months in the North to 600 mm/3months in the South. The two eastern stations appear drier than the valley ones. Conversely, CHELSA does not highlight any regional gradient but mainly orographic effects of south-facing slopes. This divergence in estimating regional gradient leads to important discrepancies between the measured rainfall amounts and CHELSA estimates. CHIRPS satellite data show a regional gradient from Northwest to Southeast. A slight orographic effect is visible on the northern slope of the Salak and on the entire Gede-Pangrango edifice. A drier zone emerges to the South of the Salak volcano which is consistent with a windward side at the north of the volcanoes, and a leeward one at the south Nevertheless, CHIRPS overestimates rainfall on the entire area (+50 to +400 mm/3months). TERRA shows mainly a west-east gradient with a gradual increase in rainfall as a function of altitude. In terms of rainfall amounts, TERRA appears the most accurate product with only slight differences (from 30 to 130 mm/3months). TERRA pattern slightly diverges from ground data but this could be due to station scarcity in the eastern and western areas.

During the wet season from December to February (DJF - Fig. 8, second row), the rainfall spatial distribution of ground data is more heterogeneous. The northern and southern parts of Salak and Gede-Pangrango volcanoes appear drier than the rest. In the valley, the rainfall amounts increase with a clear orographic effect in higher ground rain gauge (> 1400 mm/3months). CHELSA shows an increase in average rainfall mainly located on the slopes facing west, which might be due to orographic effects. This major orographic effect appears inconsistent with the ground observations. Conversely, CHIRPS and TERRA patterns are more consistent with ground data. CHIRPS highlights orographic effects concentrated in the highest area where its rainfall amounts are consistent with the few highground rain gauge. With limited rain gauges at high altitudes, it is not possible to fully validate the CHIRPS orographic pattern. In the lowest area, CHIRPS slightly overestimates rainfall amounts (from +100 mm/3months in the south to +400 mm/3months in the northern part). TERRA is underestimating orographic effects providing a quite homogenous rainfall spatial pattern. While rainfall amounts are underestimated in volcano slopes, it is overestimated in the valley and lower part.

From March to May (MAM - Fig. 8, third row), the transition season is slightly drier in the southern part and the valley. CHELSA rainfall pattern is characterized by orographic effect on southern slopes inconsistent with ground data. TERRA highlights an East-West gradient uncorrelated with the western ground station. CHIRPS provides more accurate patterns according to ground station with similar regional gradient and a foehn effect in the southern part. Nevertheless, in lowest areas CHIRPS still overestimates rainfall amounts.

Finally, during the dry season from June to August (JJA - Fig. 8, fourth row), ground data highlight a North-South regional pattern. CHELSA gridded data are characterized by southeastern influence inconsistent with ground data while TERRA and even more CHIRPS appear more reliable. In both MAM and JJA periods, it is interesting to note that CHIRPS shows a dry area in the southern part of the valley (center at 6.90°S – 106.75°E). This area, possibly related to foehn effect, appears larger on the ground data but demonstrates the ability of CHIRPS to capture such local effect.

3.2.2. Rainfall orographic gradient

The analysis of rainfall patterns highlighted the local complexity induced by mountainous environments. In order to quantify orographic effects, altitudinal gradients are determined for the 4 geo-climatic sectors. In Fig. 9, the seasons gradient for ground and product dataset are presented by average rainfall amounts for each dry (JJA) and wet (DJF) season between 2008 and 2013. During the wet season an increase in rainfall amounts in function of the elevation is visible, while during the dry season rainfall amounts and the altitudinal gradients are low. Only CHELSA highlights a slight gradient on the eastern slope of the Salak volcano. During transition periods (MAM and SON) the altitudinal gradients are in transitional states between the extremes of the dry and wet seasons.

In Pangrango's southern and northern sectors, CHELSA describes steep gradient between 400 and 800 m a.s.l. (≈77 and 60 mm/100 m for southern and northern areas, respectively). It then gradually decreases by around -12 and −13 mm/100 m for southern and northern areas. In Salak area, CHELSA gradient is more linear with variation from 13 mm/100 m in the southern part while the western slope gradient is more consistent with Pangrango slope. With a steep increase around 500 m a.s.l. of 400 mm/100 m. CHIRPS describes gradients mostly linear with an increase in orographic effects from North to South. Over the Pangrango it varies from 12 to 8 mm/100 m at southern and northern slopes respectively, while over the northern slope of the Salak it decreases to 5 mm/100 m. The lack of data on the eastern slope of Salak does not allow for an accurate gradient estimation. TERRA's data gives estimates of altitudinal gradients close to CHIRPS ones with the same trend along the north-south axis. On Pangrango, TERRA gradients vary from 9 to 7 mm/100 m between southern and northern slopes, while they decrease to 3–1 mm/100 m on northern and eastern Salak's slopes, respectively. On Salak's southern slope, TERRA data are influenced by the overestimation of the east-west gradient, which induces large rainfall amounts at low altitude.

Finally, the ground stations are represented in order to assess global product orographic effects. Unfortunately, ground rain gauges are mainly located at the base of the volcano slopes (Fig. 9). This does not allow a clear appreciation of the altitudinal gradients. In addition, these stations give local information that can be influenced by local processes such as station 6 in the center of the valley which measures rainfall amounts above the other data during the wet season (Fig. 2 and Fig. 8). The ground data are mainly consistent with the CHIRPS and TERRA data over the four sectors. CHIRPS and TERRA only overestimate rainfall on the Pangrango South area during the wet season. For CHELSA, the ground data measure lower gradients on the Pangrango while it is consistent with CHELSA on the Salak. These results once again confirm the better correlation of the ground data and CHIRPS and TERRA datasets compared to CHELSA.

4. Discussion

This study aims to assess the interest and reliability of global climate products for water management in ungauged tropical mountainous areas. The accuracy of these global products can vary spatially (Satgé et al., 2020), especially in complex areas such as tropical volcanic islands. To assess the validity of global products, we compared their rainfall estimates with ground rain gauge data,

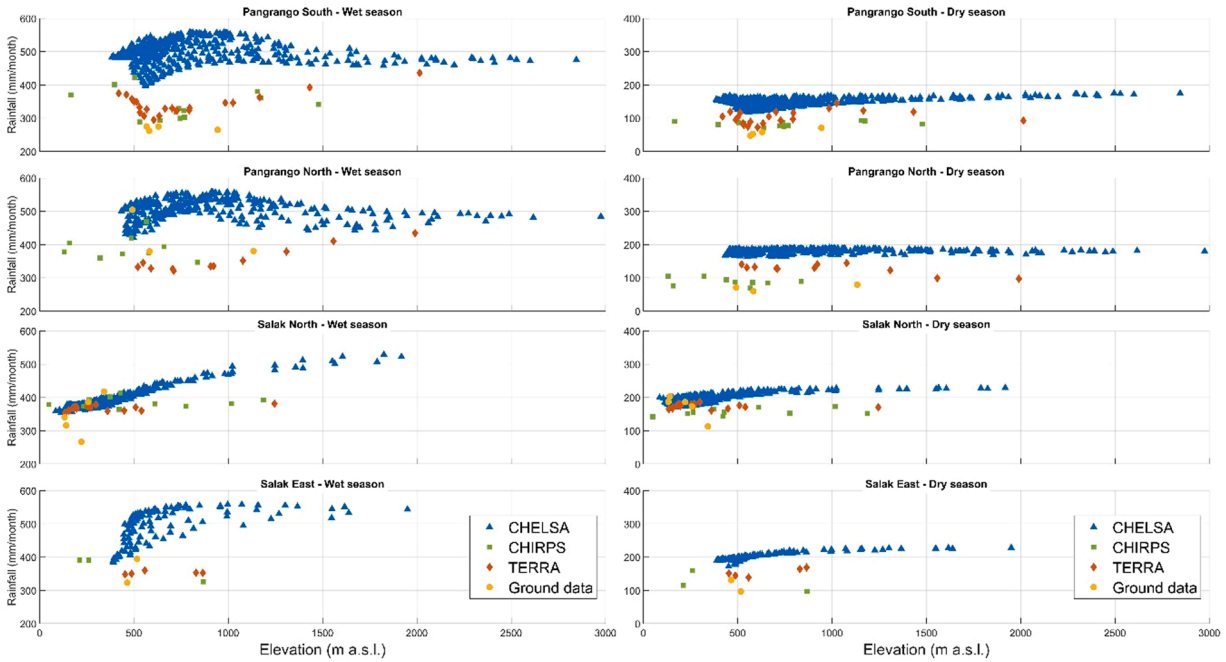

Fig. 9. Wet (DJF) and Dry (JJA) season altitudinal gradient from ground data (yellow square), CHELSA (blue triangle), CHIRPS (green square) and TERRA (orange diamond) calculated between 2008 and 2013 in mm/month. They are defined by extracting available data in the four zones defined in Fig. 3.(For interpretation of the references to colour in this figure, the reader is referred to the web version of this article.)

by analyzing both temporal and spatial patterns (Gao and Liu, 2013; Satgé et al., 2019). The direct comparison of ground data and global products is known to integrate scales effects underestimating global product scores (Tang et al., 2018).

In order to overcome such data limitation, we complete the statistical analysis with a process-based interpretation to estimate if these products are consistent according to known climatic processes in tropical mountainous contexts and with other climatic studies. These two steps provide a more exhaustive view of the strengths and weaknesses of the global products in order to properly identify whether they can be appropriate for the study area as well as their application limits. The different results are summarized in Table 4 in order to define the range of local applicability of each product for local water management.

4.1. Temporal statistical analysis

Our temporal analysis starts with a general overview of global product's performances and their spatial distribution (Figs. 4, 5). However, both climatic reanalyse and satellite data demonstrate an overestimation of rainfall amounts which is consistent with previous studies in mountaineous area (Hu et al., 2016; Hussain et al., 2018; Zeng et al., 2018). In order to assess temporal consistency, annual statistical scores are estimated. CHELSA performance decrease significantly over time, especially after 2013. However, CHIRPS and TERRA scores did not show any deteriorated nor improved temporal trends between 2002 and 2018 (Fig. 6). This result is consistent with previous studies in mountainous areas of CHIRPS dataset (e.g. Satgé et al., 2019). The variation in global product scores does not seem to be influenced by wet/dry years. Furthermore, the Indonesian climate is strongly influenced by regional climate phenomena ENSO (As-syakur et al., 2014). During the study period, El Niño events occurred in 2002, 2006, 2010, and 2015. In contrast, La Niña conditions occurred in 2007–2008 and 2011–2012 (http://www.bom.gov.au/climate/about/australian-climate-influences.shtml?bookmark=enso). The pluriannual analysis did not highlight specific patterns during these specific years. At this step, global products performance are rather constant over time demonstrating an interannual robustness.

Nevertheless, in order to set up annual water management plan, we need to correctly catch the seasonality. For short-term water management, it is mandatory to estimate the annual distribution of the recharge (mostly during the rainy season) and the importance of the drought (mostly during the dry season). These signals are generally poorly studied but are of primary importance for short-term water resource management (D'Arrigo and Wilson, 2008). Our analysis highlights a common annual pattern of global products performance (Fig. 7). During the wet season, the global products are efficient to catch rainfall amounts but underestimate the interannual variability and dynamic. During the dry season, global products tend to overestimate the rainfall while they catch the interannual variability and dynamic. Their performance decreases for transition periods and more especially between the dry and wet season. During this period, rainfall amounts and dynamics is controlled by the start of the Australian monsoon (Aldrian and Susanto, 2003). Our study highlights the issue encountered by the global products to represent efficiently this dynamics. These limitations during the dry and transition periods limit the efficiency of global products for accurate annual water management.

4.2. Spatial process-based analysis

In terms of process analysis, Fig. 9 show the variability of regional patterns and orographic effects as a function of seasonality. The ground rain gauge data shows a strong north-south regional pattern during the wet season (DFJ) and dry season (JJA). However, the distribution of ground rain gauges prevents from highlighting east-west ones. The CHELSA rainfall spatial distribution is mostly

Table 4
Summary of global product evaluation over the studied area. For the interannual and seasonal analysis, the 25% and 75% quartiles of the three statistical criteria are indicated in blue (suitable: $0.8 \leq \beta/\alpha \leq 1.2$, and $CC > 0.7$), green (average: $0.6 \leq \beta/\alpha \leq 1.4$, and $CC > 0.5$), and orange (unsuitable: poorest scores). Interannual analysis assesses the ability of global products to reproduce year-to-year variations, while seasonal analysis focuses on month-to-month variations.

		CHELSA	CHIRPS	TERRA
Interannual variability	β	1.27 - 1.46	1.17 - 1.31	1 - 1.15
	α	0.90 - 1.33	0.94 - 1.15	0.88 - 1.12
	CC	0.67 - 0.83	0.60 - 0.77	0.49 - 0.79
Seasonality	β	1.16 - 1.42	1.10 - 1.34	1.03 - 1.18
	α	0.81 – 1.15	0.82 - 1.15	0.99 - 1.15
	CC	0.59 – 0.8	0.40 - 0.66	0.22 - 0.62
Regional spatial patterns		No regional pattern	Northwest-Southeast accurate pattern	West-East regional slightly biased pattern
Foehn effect		Overestimated and inconsistent with regional circulation	Consistent with regional circulation	None
Orographic gradients		Orographic gradient overestimated	Coarse orographic gradients	Coarse orographic gradients
Global product strength		Unsuitable	Spatial variability	Temporal stability

Color code: unsuitable – average – suitable results

controlled by topography, while for TERRA, it is driven by a regional east-west pattern (Fig. 8; Table 4). These two distributions are significantly inconsistent with the ground rain gauge. In the first case, CHELSA uses the elevation and dominant winds as a proxy for rainfall interpolation (Karger et al., 2017). Our results demonstrate that the elevation is not the only factor controlling rainfall patterns as regional rainfall patterns have to be take into account. In the meantime, orographic effects strongly depends on local climate forcing and morphology limiting the accuracy of using a single rainfall-elevation relationship. In the second case, TERRA's ground data interpolation is mostly controlled by regional rainfall patterns. Orographic effects are only slightly represented with TERRA, which limits its interest for the estimation of spatial rainfall patterns (Fig. 8; Table 4). This bias could come from an insufficient consideration of orographic effects in the interpolation technique. Finally, CHIRPS relies on remote sensing data and, despite a general over-estimation of rainfall amounts, the spatial distribution appears consistent with orographic processes. CHIRPS define a north-south rainfall pattern consistent with ground data, especially with the drier area in the leeward plain at the south of the study area (Fig. 8; Table 4). Nevertheless, according to its spatial resolution, it remains impossible to assess whether CHIRPS represents correctly windward/leeward rainfall contrast.

Concerning orographic gradients, they appear to be low during most of the year over all sectors and increase during the wet season. To evaluate their accuracy, our results can be compared with two recent studies in tropical mountains. First, Toulier et al. (2019) measured an orographic gradient on the northern slope of Bromo-Tenger volcano (Java Island). At the bottom of the volcano, annual rainfall amounts quickly increase from the shore to 500–600 m a.s.l. with an altitudinal gradient around 290 mm/100 m. Between 500 and 1100 m a.s.l., the altitudinal gradient decreases nearby 100 mm/100 m. Above 1100 m a.s.l., the dynamics of the gradient is reversed, with an annual rainfall decrease between -140 to −230 mm/100 m. Second, Réchou et al. (2019) presented a detailed study of orographic effects over La Réunion Island. In tropical area, La Réunion Island climatic regime is not impacted by monsoon phenomena. Nevertheless, the study highlights strong annual altitudinal gradients between the shore and 500–700 m a.s.l. ranging from 300 to 700 mm/100 m. Above the negative altitudinal gradient induces a significant annual rainfall decrease. Finally, we estimated an increase of the altitudinal gradient in DJF season which is consistent with Réchou et al. (2019). They highlighted an altitudinal gradient increase during the wet season.

The altitudinal gradients defined by both ground and global products do not match previous studies at La Réunion Island (Réchou et al., 2019), and at Bromo-Tenger (Toulier et al., 2019), that notably show a decrease of rainfall above a given elevation (from 500 to 1100 m above the sea level). While ground rain gauges are packed at the bottom of volcano slopes, TERRA and CHIRPS present altitudinal gradients increasing with the elevation (Table 4). This bias may come from the resolution of these products (5- and 4-km pixel length, respectively), which is not fine enough to determine rainfall gradients over a 15- to 30-km long volcano. Thanks to its fine resolution, CHELSA should be able to catch such orographic effects. Nevertheless, its altitudinal gradients are too strong as they increase until 1200 to 1500 m a.s.l.Global products assessment.

Through our statistical and process-based analysis, we are able to synthesize the strengths and limitations of each of the three products. From this qualitative analysis, it is then possible to use the different global products according to their characteristics while integrating in part their uncertainties.

The first product CHELSA, a very fine spatial resolution product (1 km^2), gave limited results on both the spatial and temporal evaluation on our study area (Table 4). At the interannual time scale and even more at seasonal scale, CHELSA overestimates rainfall amounts and variability. From a spatial point of view, CHELSA is inconsistent with ground data since it relies on overestimated orographic effects. Our study demonstrates the limited interest of this product in the tropical mountainous context of our study site.

TERRA, the second product, obtains suitable and stable temporal scores (Table 4). TERRA tends to overestimate rainfall amounts during the dry season and seasonal variability during the end of the year. As this period is the driest, the related uncertainties remain acceptable for water balance computation. The east-west direction is strongly marked in the TERRA rainfall patterns compared to the ground data and orographic effects are concentrated on the summit areas limiting the interest of TERRA for spatial analysis. As it stands, TERRA should be interesting for temporal rainfall dynamics and could be a solution to coarse estimation of water balance computation. However, Terra is might be too coarse for numbers of operational water resources management applications.

The third product CHIRPS statistical scores highlights his global overestimation of rainfall, while it is mainly consistent in terms of dynamics and variability (Table 4). This overestimation could be explained by CCD bias defining warm orographic clouds into rainfall clouds (Gebregiorgis and Hossain, 2013). However, CHIRPS provides interesting results in terms of spatial patterns (Fig. 8). CHIRPS is an interesting dataset to roughly integrate spatial rainfall patterns in water management studies especially when only scarce ground rain gauges are available. Nevertheless, its resolution is too coarse to represent accurately altitudinal rainfall gradients on narrow slopes (< 15 km). CHIRPS, thus lacks efficiency for water resources management of small watersheds (<1000 km^2).

5. Conclusion

Our study aims to assess high-resolution global products accuracy for local water resources management. Their recent development opens up new solutions for water management at local scale. This integration must be complemented by a significant effort of validation at the watershed scale, especially under complex climatic behaviors. In order to overcome the limitations of ground-based data (low density of ground rain gauge, lack of river discharge data), we combined a quantitative statistical approach with a processes-based spatial analysis. The former integrates three different temporalities including the analysis of seasonal biases rarely taken into account. It allowed to discuss the general strengths and weaknesses of the global products in order to define their range of applicability for regional long-term studies. The combination with the spatial approach allows to precise the limits of each product by integrating the associated climatic processes (orientation of monsoons, orographic effect) and assess their validity for water resource management over small watersheds.

On the western part of Java, it appears difficult to select one product adapted for all the needs. Indeed, TERRA climatic reanalysis appears accurate and stable in the long term allowing to use it for water balance trends evaluations. The products are still too uncertain to effectively monitor seasonal rainfall. Nevertheless, in the absence of data, TERRA reanalysis appears the most reliable product during the whole year. For spatial analysis, it appears that only CHIRPS remote sensing data enables, among the studied products, to approach rainfall distribution. Such analysis should focus only on spatial variations due to CHIRPS overestimation, and with some necessary ground calibration.

The global products can thus be interesting locally, nevertheless their use must be conditioned in view of their weaknesses. Their temporal accuracy is interesting, but rainfall amounts bias are still too strong to be integrated in local water resources management tools. The recurrent overestimation of rainfall during the dry period hinders the intensity of droughts and the assessment of their consequences. This limitation is amplified by the difficulty of global products to capture transition period dynamics, particularly the beginning of the wet season. Spatially, satellite data provide interesting information, but the bias caused by the higher altitudes and the still coarse resolution do not allow to correctly estimate local altitudinal gradients.

CRediT authorship contribution statement

MD: conceptualization, formal analysis, investigation, data curation, writing – original draft. **MS** & **LO**: Conceptualization, validation, writing – review & editing. **PL**: validation, writing – review & editing, supervision. **BN**, **AF** & **JLB**: resources, data curation. **AM**, **H** & **ND**: project administration, funding acquisition. **VP**: project administration, funding acquisition, writing –review & editing.

Declaration of Competing Interest

The authors declare that they have no known competing financial interests or personal relationships that could have appeared to influence the work reported in this paper.

Acknowledgements

This project has been carried out within the collaboration between Sorbonne University (METIS laboratory), Water Institute by Evian, Danone Aqua group and the Universitas Padjajaran (UNPAD). This research was funded by Sorbonne University and Danone Aqua, in the framework of Danone Aqua Waterstewardship acceleration plan on watershed preservation. The authors gratefully acknowledge the significant assistance and guidance throughout this study of Jean-Carlos Ruiz, Pierre Ribstein and Agnès Ducharne (Sorbonne University – METIS laboratory).

Appendix A. Supporting information

Supplementary data associated with this article can be found in the online version at doi:10.1016/j.ejrh.2022.101037.

References

Abatzoglou, J.T., Dobrowski, S.Z., Parks, S.A., Hegewisch, K.C., 2018. TerraClimate, a high-resolution global dataset of monthly climate and climatic water balance from 1958–2015. Sci. Data 5 (1), 1–12. https://doi.org/10.1038/sdata.2017.191.

Alazzy, A.A., Lü, H., Chen, R., Ali, A.B., Zhu, Y., Su, J., 2017. Evaluation of Satellite Precipitation Products and Their Potential Influence on Hydrological Modeling over the Ganzi River Basin of the Tibetan Plateau. Adv. Meteorol. https://doi.org/10.1155/2017/3695285.

Aldrian, E., Susanto, R.D., 2003. Identification of three dominant rainfall regions within Indonesia and their relationship to sea surface temperature. Int. J. Climatol. 23 (12), 1435–1452. https://doi.org/10.1002/joc.950.

As-syakur, A.R., Adnyana, I.W.S., Mahendra, M.S., Arthana, I.W., Merit, I.N., Kasa, I.W., Ekayanti, N.W., Nuarsa, I.W., Sunarta, I.N., 2014. Observation of spatial patterns on the rainfall response to ENSO and IOD over Indonesia using TRMM Multisatellite Precipitation Analysis (TMPA). Int. J. Climatol. 34 (15), 3825–3839. https://doi.org/10.1002/joc.3939.

As-syakur, Abd R., Tanaka, T., Osawa, T., Mahendra, M.S., 2013. Indonesian rainfall variability observation using TRMM multi-satellite data. Int. J. Remote Sens. 34 (21), 7723–7738. https://doi.org/10.1080/01431161.2013.826837.

Bathelemy, R., Brigode, P., Tric, E., Boisson, D., (In Review). Rainfall in the Caribbean region: performance of four gridded datasets at the daily time step. Journal of Hydrology: Regional Studies.

Becker, A., Finger, P., Meyer-Christoffer, A., Rudolf, B., Schamm, K., Schneider, U., Ziese, M., 2013. A description of the global land-surface precipitation data products of the Global Precipitation Climatology Centre with sample applications including centennial (trend) analysis from 1901–present. Earth Syst. Sci. Data 5 (1), 71–99. https://doi.org/10.5194/essd-5-71-2013.

Chang, C.-P., Wang, Z., McBride, J., Liu, C.-H., 2005. Annual Cycle of Southeast Asia—Maritime Continent Rainfall and the Asymmetric Monsoon Transition. J. Clim. 18 (2), 287–301. https://doi.org/10.1175/JCLI-3257.1.

Charlier, J.-B., Lachassagne, P., Ladouche, B., Cattan, P., Moussa, R., Voltz, M., 2011. Structure and hydrogeological functioning of an insular tropical humid andesitic volcanic watershed: A multi-disciplinary experimental approach. J. Hydrol. 398 (3–4), 155–170. https://doi.org/10.1016/j.jhydrol.2010.10.006.

D'Arrigo, R., Wilson, R., 2008. El Niño and Indian Ocean influences on Indonesian drought: Implications for forecasting rainfall and crop productivity. Int. J. Climatol. 28 (5), 611–616. https://doi.org/10.1002/joc.1654.

Dee, D.P., Uppala, S.M., Simmons, A.J., Berrisford, P., Poli, P., Kobayashi, S., Andrae, U., Balmaseda, M.A., Balsamo, G., Bauer, P., Bechtold, P., Beljaars, A.C.M., Berg, L., van de, Bidlot, J., Bormann, N., Delsol, C., Dragani, R., Fuentes, M., Geer, A.J., Vitart, F., 2011. The ERA-Interim reanalysis: Configuration and performance of the data assimilation system. Q. J. R. Meteorol. Soc. 137 (656), 553–597. https://doi.org/10.1002/qj.828.

Dinku, T., Chidzambwa, S., Ceccato, P., Connor, S.J., Ropelewski, C.F., 2008. Validation of high-resolution satellite rainfall products over complex terrain. Int. J. Remote Sens. 29 (14), 4097–4110. https://doi.org/10.1080/01431160701772526.

Dumont, M., Reninger, P.A., Aunay, B., Pryet, A., Jougnot, D., Join, J.L., Michon, L., Martelet, G., 2021. Hydrogeophysical Characterization in a Volcanic Context From Local to Regional Scales Combining Airborne Electromagnetism and Magnetism. e2020GL092000 Geophys. Res. Lett. 48 (12). https://doi.org/10.1029/2020GL092000.

Elgamal, A., Reggiani, P., Jonoski, A., 2017. Impact analysis of satellite rainfall products on flow simulations in the Magdalena River Basin, Colombia. J. Hydrol.: Reg. Stud. 9, 85–103. https://doi.org/10.1016/j.ejrh.2016.09.001.

Fick, S.E., Hijmans, R.J., 2017. WorldClim 2: New 1-km spatial resolution climate surfaces for global land areas. Int. J. Climatol. 37 (12), 4302–4315. https://doi.org/10.1002/joc.5086.

Funk, C., Peterson, P., Landsfeld, M., Pedreros, D., Verdin, J., Shukla, S., Husak, G., Rowland, J., Harrison, L., Hoell, A., Michaelsen, J., 2015. The climate hazards infrared precipitation with stations—A new environmental record for monitoring extremes. Sci. Data 2 (1), 1–21. https://doi.org/10.1038/sdata.2015.66.

Gao, Y.C., Liu, M.F., 2013. Evaluation of high-resolution satellite precipitation products using rain gauge observations over the Tibetan Plateau. Hydrol. Earth Syst. Sci. 17 (2), 837–849. https://doi.org/10.5194/hess-17-837-2013.

Gebregiorgis, A.S., Hossain, F., 2013. Understanding the Dependence of Satellite Rainfall Uncertainty on Topography and Climate for Hydrologic Model Simulation. IEEE Trans. Geosci. Remote Sens. 51 (1), 704–718. https://doi.org/10.1109/TGRS.2012.2196282.

Gebremicael, T.G., Mohamed, Y.A., v. Zaag, P., Hagos, E.Y., 2017. Temporal and spatial changes of rainfall and streamflow in the Upper Tekezē–Atbara river basin, Ethiopia. Hydrol. Earth Syst. Sci. 21 (4), 2127–2142. https://doi.org/10.5194/hess-21-2127-2017.

Goshime, D.W., Absi, R., Ledésert, B., 2019. Evaluation and Bias Correction of CHIRP Rainfall Estimate for Rainfall-Runoff Simulation over Lake Ziway Watershed, Ethiopia. Hydrology 6 (3), 68. https://doi.org/10.3390/hydrology6030068.

Gupta, H.V., Kling, H., Yilmaz, K.K., Martinez, G.F., 2009. Decomposition of the mean squared error and NSE performance criteria: Implications for improving hydrological modelling. J. Hydrol. 377 (1), 80–91. https://doi.org/10.1016/j.jhydrol.2009.08.003.

Harris, I., Osborn, T.J., Jones, P., Lister, D., 2020. Version 4 of the CRU TS monthly high-resolution gridded multivariate climate dataset. Sci. Data 7 (1), 109. https://doi.org/10.1038/s41597-020-0453-3.

Hersbach, H., Bell, B., Berrisford, P., Hirahara, S., Horányi, A., Muñoz-Sabater, J., Nicolas, J., Peubey, C., Radu, R., Schepers, D., Simmons, A., Soci, C., Abdalla, S., Abellan, X., Balsamo, G., Bechtold, P., Biavati, G., Bidlot, J., Bonavita, M., Thépaut, J.-N., 2020. The ERA5 global reanalysis. Q. J. R. Meteorol. Soc. 146 (730), 1999–2049. https://doi.org/10.1002/qj.3803.

Hijmans, R.J., Cameron, S.E., Parra, J.L., Jones, P.G., Jarvis, A., 2005. Very high resolution interpolated climate surfaces for global land areas. Int. J. Climatol. 25 (15), 1965–1978. https://doi.org/10.1002/joc.1276.

Houze, R.A., 2012. Orographic effects on precipitating clouds. Rev. Geophys. 50 (1) https://doi.org/10.1029/2011RG000365.

Hu, Z., Hu, Q., Zhang, C., Chen, X., Li, Q., 2016. Evaluation of reanalysis, spatially interpolated and satellite remotely sensed precipitation data sets in central Asia. J. Geophys. Res.: Atmospheres 121 (10), 5648–5663. https://doi.org/10.1002/2016JD024781.

Huffman, G.J., Bolvin, D.T., Nelkin, E.J., Wolff, D.B., Adler, R.F., Gu, G., Hong, Y., Bowman, K.P., Stocker, E.F., 2007. The TRMM Multisatellite Precipitation Analysis (TMPA): Quasi-Global, Multiyear, Combined-Sensor Precipitation Estimates at Fine Scales. J. Hydrometeorol. 8 (1), 38–55. https://doi.org/10.1175/JHM560.1.

Hussain, Y., Satgé, F., Hussain, M.B., Martinez-Carvajal, H., Bonnet, M.-P., Cárdenas-Soto, M., Roig, H.L., Akhter, G., 2018. Performance of CMORPH, TMPA, and PERSIANN rainfall datasets over plain, mountainous, and glacial regions of Pakistan. Theor. Appl. Climatol. 131 (3), 1119–1132. https://doi.org/10.1007/s00704-016-2027-z.

Janowiak, J.E., Joyce, R.J., Yarosh, Y., 2001. A Real-Time Global Half-Hourly Pixel-Resolution Infrared Dataset and Its Applications. Bull. Am. Meteorol. Soc. 82 (2), 205–218. https://doi.org/10.1175/1520-0477(2001)082<0205:ARTGHH>2.3.CO;2.

Joyce, R.J., Janowiak, J.E., Arkin, P.A., Xie, P., 2004. CMORPH: A Method that Produces Global Precipitation Estimates from Passive Microwave and Infrared Data at High Spatial and Temporal Resolution. J. Hydrometeorol. 5 (3), 487–503. https://doi.org/10.1175/1525-7541(2004)005<0487:CAMTPG>2.0.CO;2.

Karger, D.N., Conrad, O., Böhner, J., Kawohl, T., Kreft, H., Soria-Auza, R.W., Zimmermann, N.E., Linder, H.P., Kessler, M., 2017. Climatologies at high resolution for the earth's land surface areas. Sci. Data 4, 170122. https://doi.org/10.1038/sdata.2017.122.

Kobayashi, S., Ota, Y., Harada, Y., Ebita, A., Moriya, M., Onoda, H., Onogi, K., Kamahori, H., Kobayashi, C., Endo, H., Miyaoka, K., Takahashi, K., 2015. The JRA-55 Reanalysis: General Specifications and Basic Characteristics. 気象集誌. 第2輯 93 (1), 5–48. https://doi.org/10.2151/jmsj.2015-001.

Körner, C., 2007. The use of 'altitude' in ecological research. Trends Ecol. Evol. 22 (11), 569–574. https://doi.org/10.1016/j.tree.2007.09.006.

Lachassagne, P., Aunay, B., Frissant, N., Guilbert, M., Malard, A., 2014. High-resolution conceptual hydrogeological model of complex basaltic volcanic islands: A Mayotte, Comoros, case study. Terra Nova 26 (4), 307–321. https://doi.org/10.1111/ter.12102.

Lestari, D.O., Sutriyono, E., Sabaruddin, S., Iskandar, I., 2018. Respective Influences of Indian Ocean Dipole and El Niño-Southern Oscillation on Indonesian Precipitation. J. Math. Fundam. Sci. 50 (3), 257–272–272. https://doi.org/10.5614/j.math.fund.sci.2018.50.3.3.

Maggioni, V., Massari, C., 2018. On the performance of satellite precipitation products in riverine flood modeling: A review. J. Hydrol. 558, 214–224. https://doi.org/10.1016/j.jhydrol.2018.01.039.

Mosier, T.M., Hill, D.F., Sharp, K.V., 2014. 30-Arcsecond monthly climate surfaces with global land coverage. Int. J. Climatol. 34 (7), 2175–2188. https://doi.org/10.1002/joc.3829.

Qian, J.-H., 2008. Why Precipitation Is Mostly Concentrated over Islands in the Maritime Continent. J. Atmos. Sci. 65 (4), 1428–1441. https://doi.org/10.1175/2007JAS2422.1.

Qian, J.-H., Robertson, A.W., Moron, V., 2010. Interactions among ENSO, the Monsoon, and Diurnal Cycle in Rainfall Variability over Java, Indonesia. J. Atmos. Sci. 67 (11), 3509–3524. https://doi.org/10.1175/2010JAS3348.1.

Réchou, A., Flores, O., Jumaux, G., Duflot, V., Bousquet, O., Pouppeville, C., Bonnardot, F., 2019. Spatio-temporal variability of rainfall in a high tropical island: Patterns and large-scale drivers in Réunion Island. Q. J. R. Meteorol. Soc. 145 (720), 893–909. https://doi.org/10.1002/qj.3485.

Satgé, F., Defrance, D., Sultan, B., Bonnet, M.-P., Seyler, F., Rouché, N., Pierron, F., Paturel, J.-E., 2020. Evaluation of 23 gridded precipitation datasets across West Africa. J. Hydrol. 581, 124412 https://doi.org/10.1016/j.jhydrol.2019.124412.

Satgé, F., Ruelland, D., Bonnet, M.-P., Molina, J., Pillco, R., 2019. Consistency of satellite-based precipitation products in space and over time compared with gauge observations and snow- hydrological modelling in the Lake Titicaca region. Hydrol. Earth Syst. Sci. 23 (1), 595–619. https://doi.org/10.5194/hess-23-595-2019.

Shrestha, N.K., Qamer, F.M., Pedreros, D., Murthy, M.S.R., Wahid, S., Md, Shrestha, M., 2017. Evaluating the accuracy of Climate Hazard Group (CHG) satellite rainfall estimates for precipitation based drought monitoring in Koshi basin, Nepal. J. Hydrol.: Reg. Stud. 13, 138–151. https://doi.org/10.1016/j.ejrh.2017.08.004.

Sobel, A.H., Burleyson, C.D., Yuter, S.E., 2011. Rain on small tropical islands. J. Geophys. Res.: Atmospheres 116 (D8). https://doi.org/10.1029/2010JD014695.

Sun, Q., Miao, C., Duan, Q., Ashouri, H., Sorooshian, S., Hsu, K.-L., 2018. A Review of Global Precipitation Data Sets: Data Sources, Estimation, and Intercomparisons. Rev. Geophys. 56 (1), 79–107. https://doi.org/10.1002/2017RG000574.

Tang, G., Behrangi, A., Long, D., Li, C., Hong, Y., 2018. Accounting for spatiotemporal errors of gauges: A critical step to evaluate gridded precipitation products. J. Hydrol. 559, 294–306. https://doi.org/10.1016/j.jhydrol.2018.02.057.

Toulier, A., Baud, B., de Montety, V., Lachassagne, P., Leonardi, V., Pistre, S., Dautria, J.-M., Hendrayana, H., Miftakhul Fajar, M.H., Satrya Muhammad, A., Beon, O., Jourde, H., 2019. Multidisciplinary study with quantitative analysis of isotopic data for the assessment of recharge and functioning of volcanic aquifers: Case of Bromo-Tengger volcano, Indonesia. J. Hydrol.: Reg. Stud. 26, 100634 https://doi.org/10.1016/j.ejrh.2019.100634.

Vittecoq, B., Fortin, J., Maury, J., Violette, S., 2020. Earthquakes and extreme rainfall induce long term permeability enhancement of volcanic island hydrogeological systems. Sci. Rep. 10 (1), 20231. https://doi.org/10.1038/s41598-020-76954-x.

Vittecoq, B., Reninger, P.-A., Lacquement, F., Martelet, G., Violette, S., 2019. Hydrogeological conceptual model of andesitic watersheds revealed by high-resolution heliborne geophysics. Hydrol. Earth Syst. Sci. 23 (5), 2321–2338. https://doi.org/10.5194/hess-23-2321-2019.

Wan, Z., 2008. New refinements and validation of the MODIS Land-Surface Temperature/Emissivity products. Remote Sens. Environ. 112 (1), 59–74. https://doi.org/10.1016/j.rse.2006.06.026.

Willmott, C.J., Robeson, S.M., 1995. Climatologically aided interpolation (CAI) of terrestrial air temperature. Int. J. Climatol. 15 (2), 221–229. https://doi.org/10.1002/joc.3370150207.

Zeng, Q., Wang, Y., Chen, L., Wang, Z., Zhu, H., Li, B., 2018. Inter-Comparison and Evaluation of Remote Sensing Precipitation Products over China from 2005 to 2013. Remote Sens. 10 (2), 168. https://doi.org/10.3390/rs10020168.